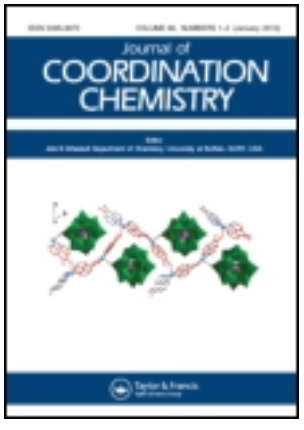

Journal of Coordination Chemistry
Publication details, including instructions for authors and subscription information:
http://www.tandfonline.com/loi/gcoo20

Dinitrogen activation by low-coordinate transition metal complexes

Aaron W. Pierpont [a] & Thomas R. Cundari [a]

[a] Department of Chemistry and Center for Advanced Scientific Computing and Modeling , University of North Texas, P.O. Box 305070 , Denton , TX 76203-5070 , USA

Published online: 06 Sep 2011.

To cite this article: Aaron W. Pierpont & Thomas R. Cundari (2011) Dinitrogen activation by low-coordinate transition metal complexes, Journal of Coordination Chemistry, 64:18, 3123-3135, DOI: 10.1080/00958972.2011.616586

To link to this article: http://dx.doi.org/10.1080/00958972.2011.616586

Journal of Coordination Chemistry
Vol. 64, No. 18, 20 September 2011, 3123–3135

Dinitrogen activation by low-coordinate transition metal complexes

AARON W. PIERPONT and THOMAS R. CUNDARI*

Department of Chemistry and Center for Advanced Scientific Computing and Modeling, University of North Texas, P.O. Box 305070, Denton, TX 76203-5070, USA

(*Received 28 June 2011; in final form 11 August 2011*)

In this article, several avenues in the ongoing computational study of first row transition metal β-diketiminate dinitrogen complexes are discussed. Analysis of monometallic N–N bond length changes reveals that upon complexation of free N_2, side-bound N_2 is 0.018–0.054 Å longer than analogous end-bound N_2. Although the same isomeric preferences across the 3-D series were calculated for bimetallic β-diketiminate N_2 complexes, the N–N bond lengths and hence N_2 activation was found to be greater compared to the monometallic species. This present research demonstrates that a useful starting point for activated dinitrogen complexes is the choice of *bimetallic* supporting ligands, which unlike monometallic ligands allow both metals to activate N_2 in a concerted fashion.

Keywords: Nitrogen activation; DFT; Catalysis

1. Introduction

The atmosphere of the Earth is composed of over 75% of a single constituent: N_2, which is used as a feedstock for the industrial synthesis of ammonia [1]. Such transformations involve the crucial step of activation and subsequent cleavage of the N≡N bond of dinitrogen. This process is facile for naturally occurring *nitrogenases*, where activation takes place at Fe–Mo–S clusters (FeMo cofactor or ''FeMoCo'') [2], which have spurred the development of artificial analogs. The first industrial scale method, which still enjoys almost exclusive use in ammonia production, is the Haber–Bosch process. However, given the high thermodynamic and kinetic stabilities of dinitrogen, this process requires temperature and pressure ranging from 400°C to 500°C and 100–300 atm, respectively [3]. Active research in this area has thus shifted toward the development of low temperature/pressure transition metal catalysts to activate dinitrogen.

In light of the presence of Fe–Mo clusters in the active sites of most *nitrogenases*, development of synthetic analogs has proceeded in a mimetic fashion toward both Fe and Mo complexes. Although there are numerous examples of N_2 cleavage reported for Mo–N_2 complexes [4], due in large part to the strength of the resulting Mo≡N bonds,

*Corresponding author. Email: t@unt.edu

ISSN 0095-8972 print/ISSN 1029-0389 online © 2011 Taylor & Francis
DOI: 10.1080/00958972.2011.616586

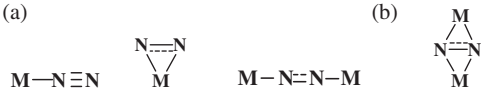

Scheme 1. (a) Mono- and (b) bimetallic N_2 binding modes.

most Fe–N_2 complexes reported to date are coordinatively saturated at the metal center with the bound N_2 ligand displaying minimal activation (typically judged by N–N bond length and stretching frequencies) with respect to free N_2 [5]. Fortunately, recent DFT and multi-configurational self-consistent field [6] computations for LFeNNFeL complexes (L = β-diketiminate) have suggested several plausible routes for achieving greater N_2 activation (defined herein as N–N bond lengthening with respect to free N_2), in similar complexes: (i) low Fe coordination numbers, (ii) reduction of the LFeNNFeL complexes with alkali metals, (iii) variation of substituents around the β-diketiminate periphery, (iv) two β-diketiminate fragments as opposed to one, and (v) increased population of FeN π and NN π^* molecular orbitals [7]. In this report, we explore the effect of first row transition metal (Sc–Cu) on N_2 activation in mono- and bimetallic β-diketiminate complexes.

Additionally, the particular binding mode of dinitrogen in TM–N_2 complexes can have important ramifications for N_2 activation. For the earliest reported (1965) dinitrogen complex, $[Ru(NH_3)_5N_2]^{2+}$, N_2 is bound to Ru in an end-on (κ^1) fashion [8]. Throughout the following decades, research on similar κ^1–N_2 complexes was directed toward reactivity with dinitrogen and electrophiles. Only after the discovery of the first planar side-on (η^2) f-block dinitrogen complex $(Cp^*_2Sm)_2(\mu$–$\eta^2:\eta^2$–$N_2)$ did the synthesis and reactivity of novel η^2–N_2 complexes gain momentum [9]. Additionally, in a recent review, MacLachlan and Fryzuk [10] found two salient features of relevance to this research regarding N_2 binding modes. First, η^2–N_2 complexes display greater activation than any κ^1–N_2 complex to date. Second, of the d- and f-block dinitrogen complexes considered by the authors, the side-on complexes of the former subset were in general more activated. Thus, in addition to the aforementioned N_2 activation enhancement routes, end-on (κ^1) and side-on (η^2) isomers of select N_2 complexes will be addressed in this report. Pertinent binding modes are illustrated in scheme 1 for both mono- and bimetallic complexes.

2. Monometallic (β-diket)M–NN complexes

The effect of first row transition metal (M: Sc–Cu) on activation in (β-diket)M–N_2 complexes was modeled. It was initially supposed that, for certain transition metals, the η^2–N_2 isomer would be more stable than κ^1–N_2 isomer, scheme 1, and in other cases the linkage isomer preferences might be reversed. This supposition is in fact supported by the data in figure 1, where [M] = (β-diket)M.

The geometry about Sc in both ^{3}[Sc]–N_2 isomers is Y-shaped (figure 2 (top)). The ^{3}[Sc]–(κ^1–N_2) complex is slightly pyramidal about Sc (sum of angles at Sc = 345.37°) with an N–N distance of 1.144 Å, whereas that in the more stable ^{3}[Sc]–(η^2–N_2) isomer is 1.171 Å, the largest among the [M]–N_2 series (Sc–Cu). By contrast, both ^{4}[Ti]–(κ^1–N_2)

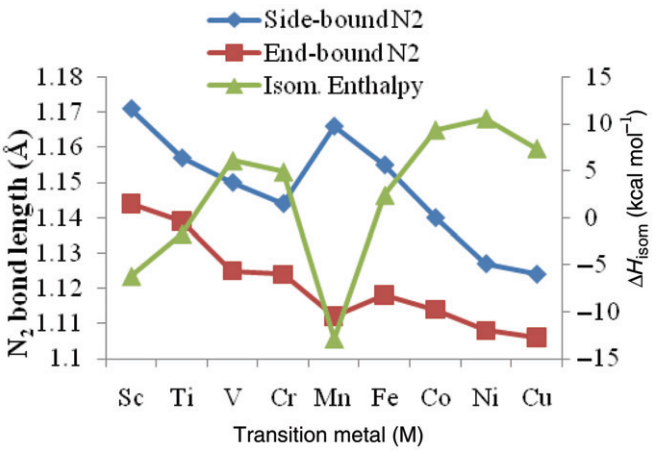

Figure 1. N_2 bond lengths (left axis) and isomerization enthalpies (right axis) for monometallic [M]–N_2 complexes.

and ^{4}[Ti]–(η^2–N_2)* ($\Delta H_{gap}(2/4) = 5.2$ kcal mol^{-1}; the excited state [Ti]–(η^2–N_2)* bond length has been reported in order to give a spin-allowed N_2 isomerization) are T-shaped (figure 2 (middle)) with N_2 bond lengths 1.139 Å and 1.157 Å, respectively. Based on the average N_2 bond lengths of terminal κ^1–Ti–N_2 complexes in the Cambridge Structural Database (CSD) [11] (N–N: 1.110 ± 0.006 Å; $N = 5$), B3LYP may overestimate the N–N distance (1.139 Å) in ^{4}[Ti]–(κ^1–N_2), although this discrepancy may arise from the absence of experimentally characterized three-coordinate Ti–N_2 complexes. The largest N–Ti–N(N_2) angles (''Tee'' angles) are 167.79° (κ^1–N_2) and 161.29° (η^2–N_2), where the Tee angle N–Ti–N(N_2) is measured with respect to the midpoint of the N_2 unit.

The geometry of the Y-shaped ^{5}[V]–(η^2–N_2) isomer is similar to ^{3}[Sc]–(η^2–N_2), with an N_2 bond length of 1.150 Å, in contrast to the more stable T-shaped ^{5}[V]–(κ^1–N_2) isomer ($\Delta H_{isom} = 6.1$ kcal mol^{-1}; Tee angle: 170.41°; N–N: 1.125 Å). The calculated N_2 bond length in the κ^1 isomer (1.125 Å) is in excellent agreement with that of each terminal N_2 (1.130(16) Å) in [Na(THF)][V(N_2)$_2$(dppe)$_2$] (dppe = $Ph_2PCH_2CH_2PPh_2$) [12], the lone V–N_2 complex in the CSD. Both isomers of ^{6}[Cr]–N_2 are Y-shaped, with a shorter N_2 bond length in the more stable ($\Delta H_{isom} = 4.9$ kcal mol^{-1}) κ^1–N_2 isomer (N–N: 1.124 Å (κ^1); 1.144 Å (η^2)). Again, excellent agreement is found between this N_2 bond length and those of the single terminal Cr–N_2 structure in the CSD (1.122(3) Å), *trans*-Cr(N_2)$_2$(dmpe)$_2$ (dmpe = $(CH_3)_2PCH_2CH_2P(CH_3)_2$) [13].

From Sc–Cr, N_2 bond lengths in either end-on or side-on isomers decrease monotonically from 1.144 Å to 1.124 Å and 1.171 Å to 1.144 Å, respectively. On the other hand, an increase from −6.2 to 6.1 kcal mol^{-1} in ΔH_{isom} is found on moving from ^{3}[Sc]–N_2 to ^{5}[V]–N_2, with a slight decrease from V to Cr ($\Delta H_{isom} = 4.9$ kcal mol^{-1}). *Thus, for these systems (Sc–Cr), the η^2–N_2 isomer exhibits greater activation for the earliest TM systems and is most stable for Sc and Cr*. However, there is an abrupt break in the η^2–N–N (1.166 Å) and ΔH_{isom} (−12.9 kcal mol^{-1}) trends for the Y-shaped ^{5}[Mn]–N_2 complexes (figure 1). This anomalous behavior may reflect deficiencies of B3LYP, which may also be reflected in poor agreement between the N_2 bond length in the less stable ^{5}[Mn]–(κ^1–N_2) isomer (1.112 Å) and that in the lone terminal Mn–N_2 complex in the CSD, MnH(N_2)(dmpe)$_2$ (1.127(7) Å) [14].

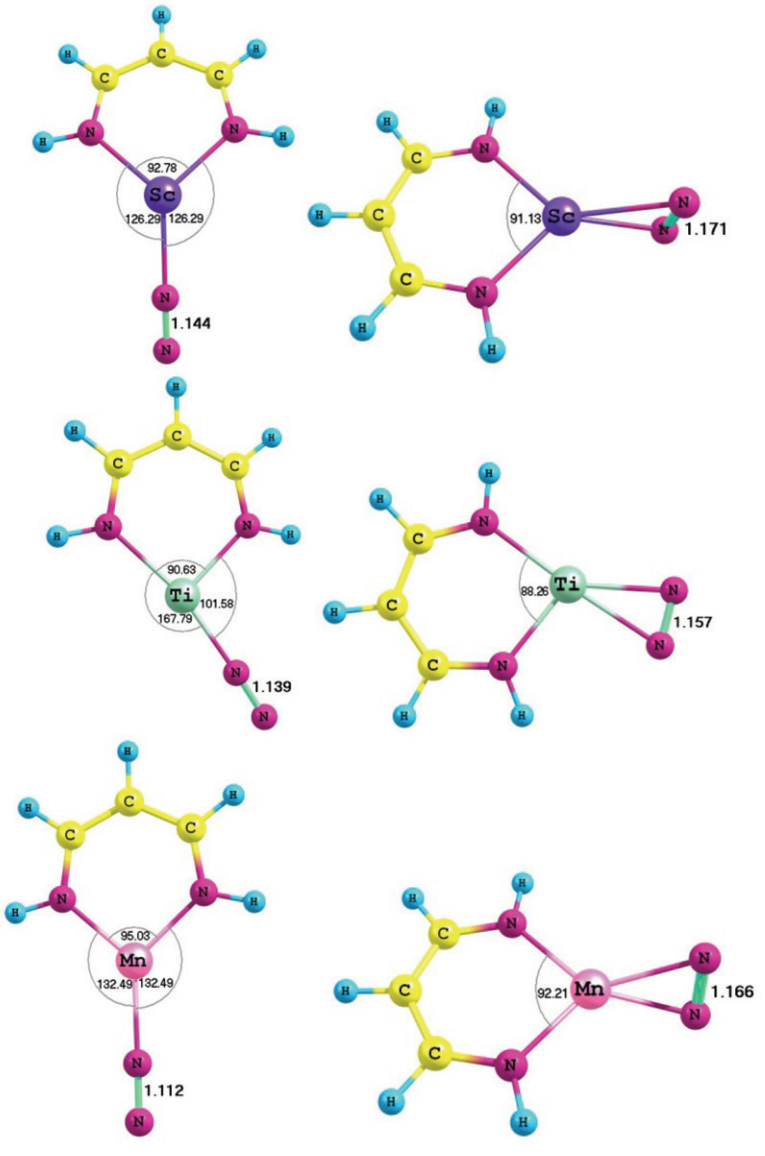

Figure 2. Geometries of end-on (κ^1) and side-on (η^2) ^{3}[Sc]–N_2 (top), ^{4}[Ti]–N_2 (middle), and ^{5}[Mn]–N_2 complexes (bottom). N_2 bond lengths (**bold**) in Å and bond angles in degrees.

For Fe–N_2 complexes, side-bound ^{4}[Fe]–(η^2–N_2) is Y-shaped with an N_2 bond length of 1.155 Å. Within the more stable T-shaped ($\Delta H_{isom} = 2.4$ kcal mol^{-1}; Tee angle: 165.70°; section 2.1) ^{4}[Fe]–(κ^1-N_2) complex, the N–N distance of 1.118 Å is consistent with that of the 27 terminal Fe–N_2 complexes in the CSD (1.111 ± 0.023 Å). Like the Fe complexes, the more stable end-on ^{3}[Co]–(κ^1–N_2) is T-shaped ($\Delta H_{isom} = 9.4$ kcal mol^{-1}; N–N: 1.114 Å) whereas the side-on ^{3}[Co]–(η^2–N_2) is Y-shaped (N–N: 1.140 Å). The N–N distance in the former complex (1.114 Å) lies slightly higher than the average of those in the eight terminal Co–N_2 complexes in the CSD (1.100 ± 0.012 Å).

As with the Ti–N_2 complexes, the ^{2}[Ni]–(κ^1–N_2) and ^{2}[Ni]–(η^2–N_2) complexes are T-shaped (Tee angles: 161.91° and 155.35°, respectively) with a shorter N_2 bond length in the more stable κ^1 isomer (N–N: 1.108 Å; $\Delta H_{isom} = 10.6\,kcal\,mol^{-1}$) than in the side-bound isomer (N–N: 1.127 Å). The N–N distance in ^{2}[Ni]–(κ^1–N_2) is in excellent agreement with that in the terminal Ni–N_2 complex (dtbpe)Ni(N_2)(PPh_3) (N–N: 1.112(2) Å; dtbpe = P(^{t}Bu)$_2$CH$_2$CH$_2$P(^{t}Bu)$_2$) [15]. Finally, the two ^{1}[Cu]–N_2 complexes are Y-shaped, where the κ^1–N_2 isomer is thermodynamically favored ($\Delta H_{isom} = 7.4\,kcal\,mol^{-1}$). For each isomer, the N–N distances in the Cu complexes (1.106 Å (κ^1–N_2) and 1.124 Å (η^2–N_2)) are the shortest among their respective first row TM counterparts (figure 1). Like Sc, no terminal Cu–N_2 complexes have been reported experimentally.

From Mn–Cu, the η^2–N–N distances decrease monotonically from 1.166 to 1.124 Å with concomitant increase in ΔH_{isom} (although a slight decrease from Ni ($10.6\,kcal\,mol^{-1}$) to Cu ($7.4\,kcal\,mol^{-1}$) was calculated). Although the η^2–N_2 isomer is most stable for [Mn], the remaining late 3-D systems (Fe–Cu) show a thermodynamic preference for the κ^1–N_2 isomer, whose N_2 bond lengths display relatively little sensitivity to TM (1.118–1.106 Å). *Thus, from the data presented graphically in* figure 1, *earlier [M]–N_2 complexes, with either κ^1– or η^2–N_2 isomers, exhibit greater N_2 activation than later systems within the two 3-D sets (Sc–Cr and Mn–Cu) partitioned by the "jump" between Cr and Mn*. Furthermore, the η^2–N_2 isomer is most stable in the earliest 3-D [M]–N_2 complexes (M = Sc, Ti, Mn). Nevertheless, given the paucity of monometallic [M]–(η^2–N_2) complexes in the CSD, the foregoing analysis must be expanded to bimetallic systems for which *bona fide* examples of η^2–N_2 isomers have been reported.

3. Bimetallic (*β*-diket)M–NN–M(*β*-diket) complexes

Unlike the monometallic complexes (figure 1), the corresponding trends in N–N bond lengths and κ^1/η^2–N_2 isomer stability (ΔH_{isom}) for bimetallic complexes [M]–NN–[M], figure 3, are much smoother, almost monotonic, where low-lying excited state κ^1–N_2 bond lengths have been reported for Sc and V in order to give spin-allowed N_2 isomerizations (ΔH_{isom}). For Sc, the η^2 isomer ^{1}[Sc]–(η^2–N_2)–[Sc] was most stable owing to thermodynamically favorable isomerization ($\Delta H_{isom} = -44.4\,kcal\,mol^{-1}$) from ^{1}[Sc]–($\kappa^1$–$N_2$)–[Sc]* ($\Delta H_{gap}(5/1) = 1.9\,kcal\,mol^{-1}$). There is marked difference in the optimized geometries of the ground-state quintet (^{5}[Sc]–(κ^1–N_2)–[Sc]) and low-lying singlet excited state (^{1}[Sc]–(κ^1–N_2)–[Sc]*), shown in figure 4. The latter complex is highly pyramidal about each Sc with Sc–N(N_2) and N–N 1.851 Å and 1.274 Å, respectively (figure 4), whereas planar Sc environments and substantially longer Sc–N(N_2) (2.056 Å) and shorter N–N (1.208 Å) distances were found in the former (figure 4). However, the ground state ^{1}[Sc]–(η^2–N_2)–[Sc] complex features a very long N_2 bond (1.512 Å), the longest among the [M]–(κ^1–N_2)–[M] and [M]–(η^2–N_2)–[M] 3-D series (figure 3), with the N–N axis perpendicular to each *β*-diketiminate Sc plane (figure 4). This N_2 bond is 0.05 Å longer than the 1.46 Å N–N single bond in the X-ray crystal structure of hydrazine (H_2N–NH_2) [16].

As with Sc, the side-bound N_2 isomer (^{3}[Ti]–(η^2–N_2)–[Ti]) is thermodynamically preferable ($\Delta H_{isom} = -26.4\,kcal\,mol^{-1}$) to the end-on isomer (^{3}[Ti]–(κ^1–N_2)–[Ti]) in the bimetallic Ti complexes. Other than a T-shaped geometry (Tee angle = 148.35°) the

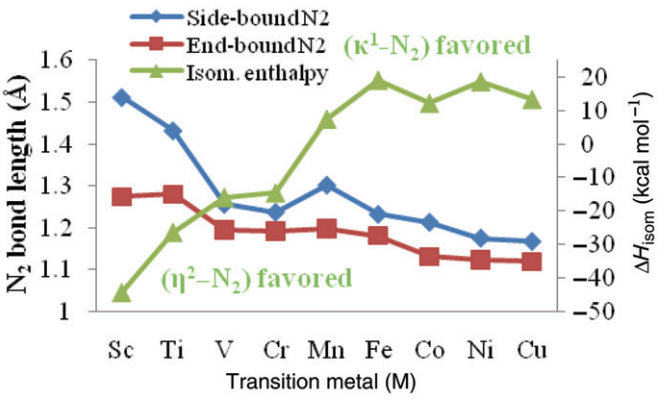

Figure 3. N_2 bond lengths (left axis) and isomerization enthalpies (right axis) for bimetallic [M]–N_2–[M] complexes.

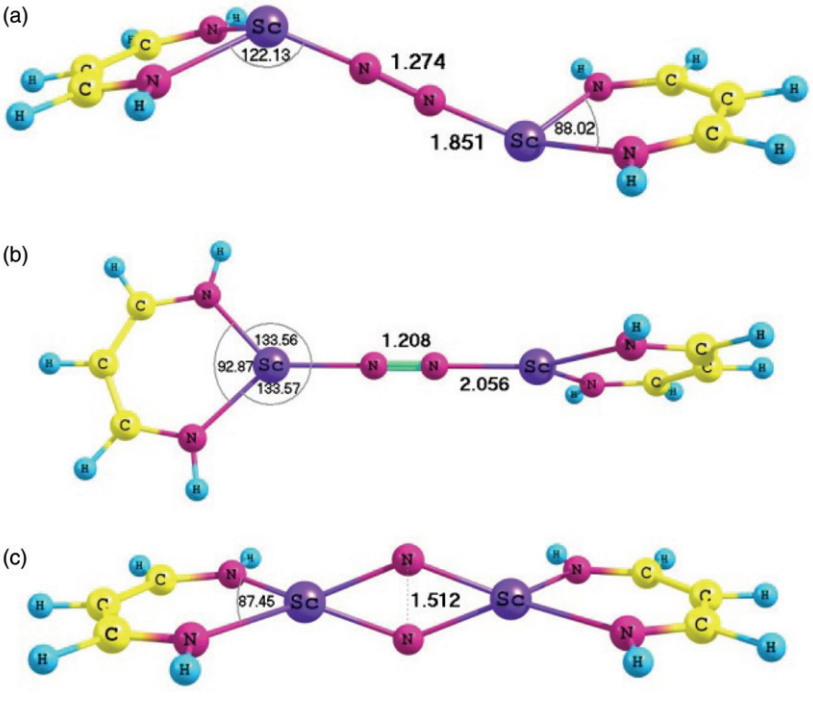

Figure 4. Optimized geometries of (a) ^{1}[Sc]–(κ^1–N_2)–[Sc]*, (b) ^{5}[Sc]–(κ^1–N_2)–[Sc], and (c) ^{1}[Sc]–(η^2–N_2)–[Sc]. Sc–N and N–N bond lengths (**bold**) in Å and all angles in degrees.

structure of the latter complex is similar to that of ^{1}[Sc]–(κ^1–N_2)–[Sc]* (figure 4), with a 1.280 Å N–N distance. Nevertheless, the Y-shaped geometry of ^{1}[Sc]–(κ^1–N_2)–[Sc]* is reproduced in the low-lying ($\Delta H_{isom} = 1.0$ kcal mol^{-1}) septet ^{7}[Ti]–(κ^1–N_2)–[Ti]* structure, with a shorter N–N bond length (1.195 Å). In fact, repeating the optimizations of

these two end-on complexes with the more accurate [17] B1B95 functional [18] reversed the order of these spin states, yielding a ground-state κ^1 septet (N–N: 1.190 Å) structure lying only 0.16 kcal mol^{-1} *below* the triplet. Consequently, we believe that the spin states in the κ^1–N_2 complexes are improperly ordered at the B3LYP/6-311 + G(d) level of theory, giving rise to the slight increase in N_2 bond length from ^{1}[Sc]–(κ^1–N_2)–[Sc]* (1.274 Å) to ^{3}[Ti]–(κ^1–N_2)–[Ti] (1.280 Å; figure 4).

A search of the CSD [14] returned 23 structures bearing κ^1–Ti–N_2–Ti motifs with an average N_2 bond length of 1.208 ± 0.054 Å. Although this experimental average is in closer agreement with the B1B95 value for ^{7}[Ti]–(κ^1–N_2)–[Ti] (N–N: 1.190 Å), three of the CSD structures exhibited N_2 bond lengths in excess of the B3LYP value (1.280 Å). In contrast, the calculated N_2 bond lengths in ^{3}[Ti]–(η^2–N_2)–[Ti] (1.410 (B1B95) and 1.432 (B3LYP) Å, respectively) significantly overestimate the two CSD values for η^2–Ti–N_2–Ti motifs (1.380 Å and 1.216 Å), and are in fact closer to the average for the 14 CSD η^2–Zr–N_2–Zr structures (1.445 ± 0.104 Å).

Continuing the trend found in the previous Sc and Ti systems, a low-lying excited state ^{7}[V]–(κ^1–N_2)–[V]* complex was found ($\Delta H_{gap}(9/7) = 1.1$ kcal mol^{-1}) above the ^{9}[V]–(κ^1–N_2)–[V] ground state. The structure of the latter complex is similar to that of ^{5}[Sc]–(κ^1–N_2)–[Sc] (figure 4), albeit with a shorter N–N distance (1.183 Å), whereas the former complex features T-shaped, slightly pyramidal V environments (figure 5a) and a slightly more activated N_2 unit (1.195 Å) over that in the ground state. In either case, both bond lengths are much shorter than the average for the 12 CSD κ^1–V–N_2–V complexes (1.243 ± 0.016 Å). The side-on complex (^{7}[V]–(η^2–N_2)–[V]) is again more stable ($\Delta H_{isom} = -15.9$ kcal mol^{-1}), with a structure similar to those of the end-on Sc and Ti complexes and a 1.256 Å N_2 bond length. Although N_2 is not cleaved in this complex as was found experimentally for $[V(N\{N''\}_2)Cl]_2$ ($[(N\{N''\}_2] = [(Me_3Si)N\text{-}\{CH_2CH_2N(SiMe_3)\}_2]$) upon reducing with KC_8 and N_2 to give the bridged nitrido complex $[V(N\{N''\}_2)(\mu\text{–}N)]_2$ (N–N: 2.50(2) Å) [19], the N–N bond length is in excellent agreement with that of the N = N double bond (1.252 Å) in the X-ray structure of diazene [20], which implies that [V]–NN–[V] complexes reduce N_2 to a double bond.

Nonet ground states were found for both Cr isomers (^{9}[Cr]–(κ^1–N_2)–[Cr] and ^{9}[Cr]–(η^2–N_2)–[Cr]), with the side-bound N_2 complex again most stable ($\Delta H_{isom} = -14.6$ kcal mol^{-1}). Unlike the earlier bimetallic κ^1–N_2 complexes, in which both β-diketiminate rings are mutually perpendicular (*cf*. figures 4 and 5), the rings in ^{9}[Cr]–(κ^1–N_2)–[Cr] are coplanar (figure 5b), where the N_2 bond length (1.191 Å) is within one standard deviation of the three CSD values for κ^1–Cr–N_2–Cr complexes (1.177 ± 0.066 Å). The two β-diketiminate rings are also planar in ^{9}[Cr]–(η^2–N_2)–[Cr] (figure 5c), in which the N–N bond length of 1.237 Å is in excellent agreement with the single CSD value (1.249 Å) for η^2–Cr–N_2–Cr complexes. This is unsurprising, given that the system in question ([{N(2,6-di-isopropyl-phenyl)C(CH_3)}$_2$CHCr]$_2$(μ-N_2)) [21] is merely a bulkier analog of the β-diketiminate complexes considered in this study. However, Monillas [21] measured an effective magnetic moment μ_{eff} of 3.9 μ_B per Cr center, consistent with a septet ground state ($S = 3$) as opposed to the calculated nonet ground state for the η^2 model system.

Both [Mn]–NN–[Mn] isomers are nonets (^{9}[Mn]–(κ^1–N_2)–[Mn] and ^{9}[Mn]–(η^2–N_2)–[Mn]). In contrast to earlier metals, the most stable isomer is now the former *end-on* complex ($\Delta H_{isom} = 7.4$ kcal mol^{-1}). This behavior is in contrast to the monometallic analogs (figures 1 and 3), for which a "dip" in ΔH_{isom} was found. Along with a 1.302 Å N–N bond length, the geometry of the less stable ^{9}[Mn]–(η^2–N_2)–[Mn] complex

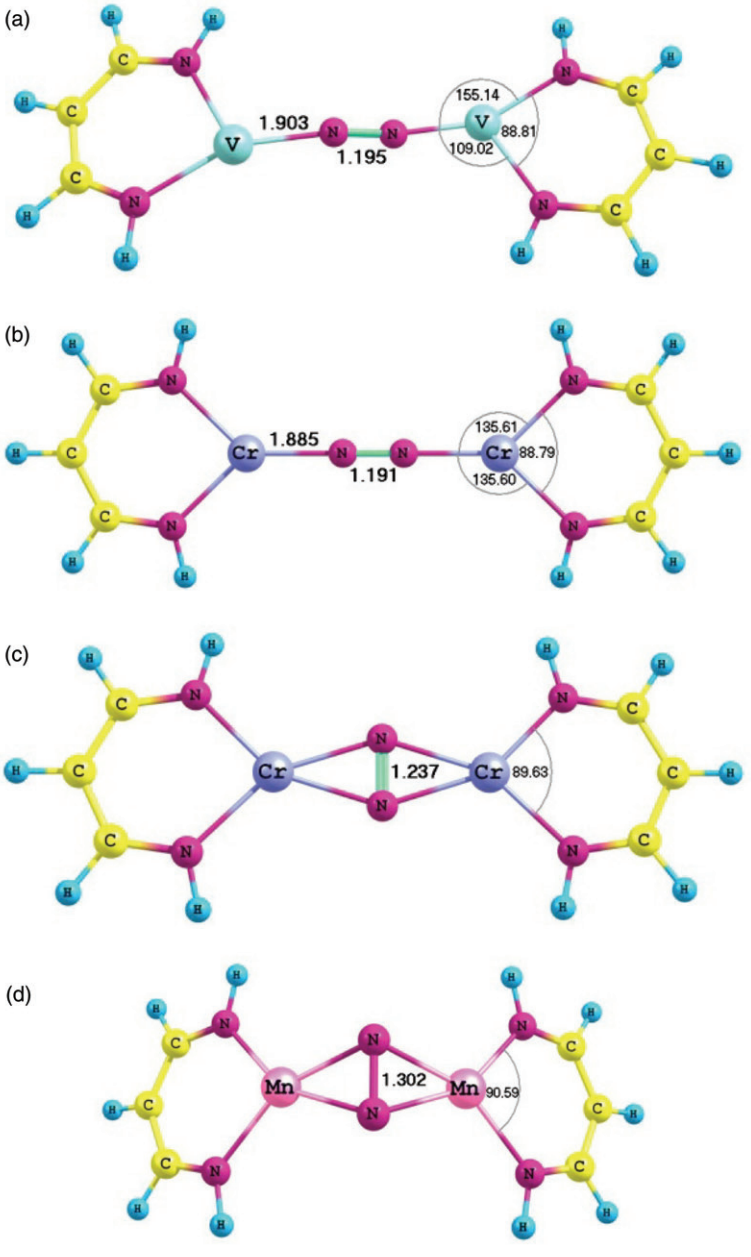

Figure 5. Optimized geometries of (a) ^{7}[V]–(κ^1–N_2)–[V]*, (b) ^{9}[Cr]–(κ^1–N_2)–[Cr], (c) ^{9}[Cr]–(η^2–N_2)–[Cr], and (d) ^{9}[Mn]–(η^2–N_2)–[Mn]. Bond lengths (**bold**) in Å and all angles in degrees.

(figure 5d) features an interesting ''butterfly'' motif, where the angle between the two Mn–N_2 planes (''butterfly angle''; *cf.* figure 5) is 130.3° and gives rise to a ''kink'' in the graph of η^2–N_2 bond length *versus* transition metal (figure 3). The N–N bond length in the κ^1–N_2 isomer (1.197 Å) is in good agreement with that in the end-bound

$([N_2P_2]Mn)_2(\mu\text{–}N_2)$ complex [22] (N–N: 1.208 Å; $[N_2P_2] = {}^t$BuNSiMe$_2$N(CH$_2$CH$_2$P^{i}Pr$_2$)$_2$), the only crystallographically characterized Mn–dinitrogen complex to date.

Thus far (*M: Sc–Mn*), *the N_2 activation trends in bimetallic* [*M*]–*NN*–[*M*] *complexes mirror those for their monometallic counterparts* ([*M*]–N_2; figure 1), *whereby weaker N–N bonds are calculated for earlier transition metal systems*. However, previous experimental work in conjunction with theoretical calculations from our group has shown the ability to weaken N_2 to be correlated with occupation of high-energy d-orbitals which in turn donate electrons to N–N π^* orbitals [23–25]. It is therefore natural to determine the extent to which this weakening ability can curtail the trend of decreasing N_2 activation from Sc–Mn in the Fe–Cu transition metal analogs, whose corresponding d-orbitals lie lower in energy.

A septet (^{7}[Fe]–(κ^1–N$_2$)–[Fe]) and quintet (^{5}[Co]–(κ^1–N$_2$)–[Co]) ground state was found for the optimized geometries of the Fe and Co complexes, respectively, figure 6 [24]. Relevant bond lengths of selected species are shown in table 1. The optimized ^{7}[Fe]–(κ^1–N$_2$)–[Fe] structure displays a Y-shaped geometry (local C_{2v} symmetry) about each Fe as well as Fe–N (1.771 Å expt.; 1.801 Å calcd) and N–N (1.189 Å expt.; 1.181 Å calcd) bond lengths, in good agreement with the previously determined L$^{t\text{Bu}}$FeNNFeL$^{t\text{Bu}}$ X-ray crystal structure [25]. Surprisingly, even though the triplet ^{3}[Co]–(κ^1–N$_2$)–[Co] was calculated to lie 10.5 kcal mol^{-1} above the corresponding ground state quintet, the triplet geometry most closely conforms to that of the X-ray crystal structure. Most significantly, the geometry about the Co center is distorted toward a T-shape (“Tee-angle”: 162.0(2)° expt.; 164.24° ave. calcd) and the Co–N (1.840 Å expt.; 1.827 Å ave. calcd) and N–N (1.139 Å expt.; 1.131 Å calcd) bond lengths are in good agreement. By contrast, the ^{5}[Co]–(κ^1–N$_2$)–[Co] structure exhibits a Y-shaped geometry (local C_{2v} symmetry) about each Co and the pertinent bond lengths (Co–N: 1.786 Å; N–N: 1.169 Å) show greater disparity with respect to those of the crystal structure. Additionally, NMR experiments [24] suggest an effectively C_{2v} structure in solution, implying that the Y and T isomers are close in energy.

The remaining bimetallic 3-D [M]–(κ^1–N$_2$)–[M] complexes are those of Ni and Cu. Geometry optimizations yielded a triplet ^{3}[Ni]–(κ^1–N$_2$)–[Ni] and singlet ^{1}[Cu]–(κ^1–N$_2$)–[Cu] ground state for the Ni and Cu species, respectively, figure 6. Subsequently, the corresponding side-on [M]–(η^2–N$_2$)–[M] models were optimized, giving the same ground state in both isomers (^{7}[Fe]–(η^2–N$_2$)–[Fe], ^{5}[Co]–(η^2–N$_2$)–[Co], ^{3}[Ni]–(η^2–N$_2$)–[Ni], and ^{1}[Cu]–(η^2–N$_2$)–[Cu]). The side-on isomers for Fe–Ni are shown in figure 6 with calculated N–N bond lengths and ΔH_{isom} values given in table 1.

The ^{7}[Fe]–(η^2–N$_2$)–[Fe] side-on N_2 complex (figure 6a) is entirely planar with approximate D_{2h} symmetry and a calculated N–N bond length of 1.232 Å (elongated by 0.051 Å and 0.136 Å with respect to the end-on isomer and free N_2, respectively), a value similar to that in the early ^{9}[Cr]–(η^2–N$_2$)–[Cr] complex (1.237 Å). Despite this encouraging result, the complex also bears a relatively high isomerization enthalpy (19.1 kcal mol^{-1}). The structure of ^{5}[Co]–(η^2–N$_2$)–[Co] (figure 6b), by contrast, shows a “butterfly” motif with a 113.82° butterfly angle, in addition to mutually perpendicular β-diketiminate planes. Although the N–N bond length of 1.213 Å is slightly smaller than that in the side-bound Fe complex, it is less elongated by 0.044 Å with respect to the end-on isomer, which may explain in part the lower isomerization enthalpy of 11.1 kcal mol^{-1}.

The optimized side-on geometry of the ^{3}[Ni]–(η^2–N$_2$)–[Ni] complex (figure 6c) is remarkable. Not only does the complex have a butterfly angle of 119.78° for its central

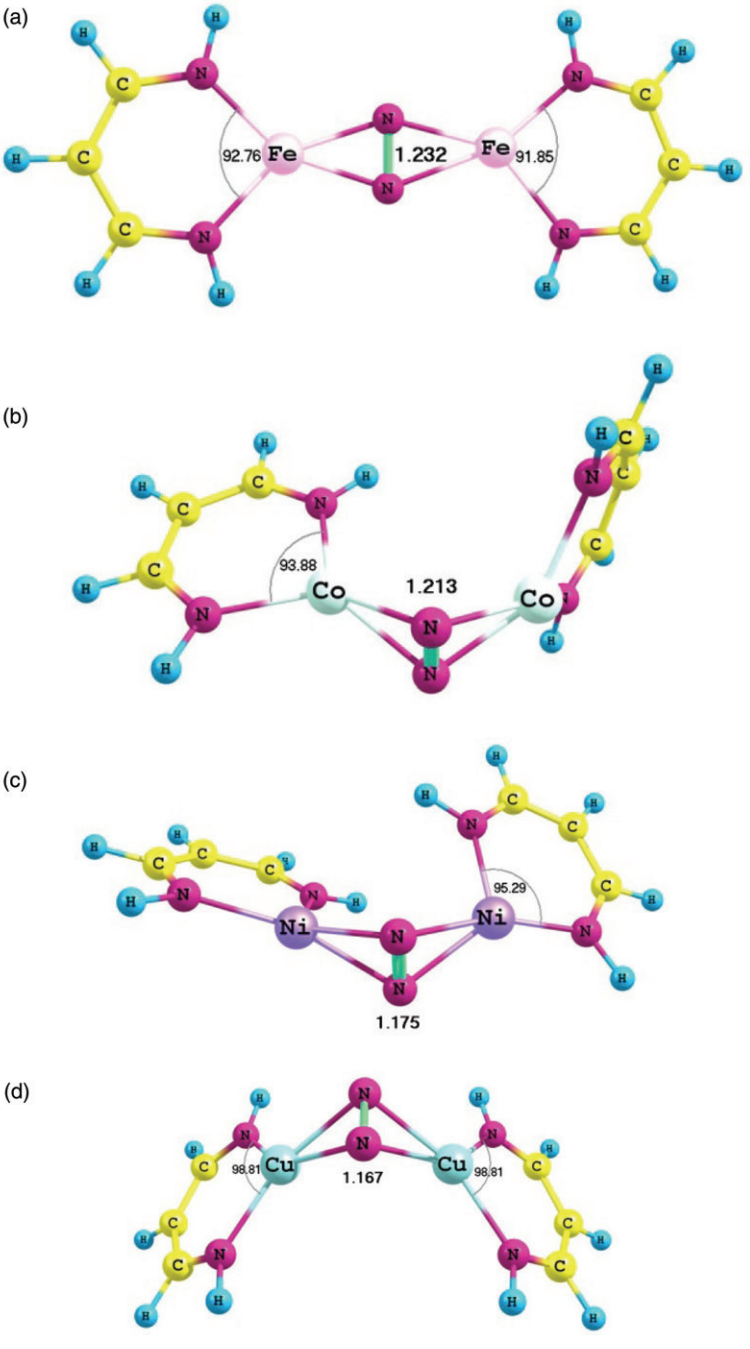

Figure 6. Optimized geometries of (a) ^{7}[Fe]–(η^2–N_2)–[Fe], (b) ^{5}[Co]–(η^2–N_2)–[Co], (c) ^{3}[Ni]–(η^2–N_2)–[Ni], and (d) ^{1}[Cu]–(η^2–N_2)–[Cu]. N_2 bond lengths (**bold**) in Å and all angles in degrees.

Table 1. Effect of late transition metal (M=Fe–Cu) on N–N bond length and ΔH_{isom} in optimized [M]–NN–[M] complexes (figure 6).[a]

	κ^1–N_2		η^2–N_2		
	N–N	Δ(N–N)[b]	N–N	Δ(N–N)[b]	ΔH^c_{isom}
^{7}LFeNNFeL	1.181	0.085	1.232	0.136	19.1
^{5}LCoNNCoL	1.169	0.073	1.213	0.117	11.1
^{3}LNiNNNiL	1.124	0.028	1.175	0.079	18.6
^{1}LCuNNCuL	1.119	0.023	1.167	0.071	13.3

[a]Bond lengths in Å and enthalpies in kcal mol^{-1}.
[b]Difference in calculated N_2 bond length in complex and free N_2 (1.096 Å).
[c] ΔH_{isom}: $\kappa^1-N_2 \rightarrow \eta^2-N_2$.

Ni_2N_2 motif similar to that of Co_2N_2, it also exhibits approximate C_2 symmetry about an axis passing through the center of the bound N_2 molecule and lying in a plane bisecting the butterfly angle. The N–N bond length of 1.124 Å in the end-on Ni isomer becomes elongated by 0.051 Å to 1.175 Å in the side-on isomer with an isomerization enthalpy of 18.6 kcal mol^{-1}. The end-on isomer is most directly comparable to the structure reported by Pfirrmann and coworkers [26]. To wit, agreement between theory and experiment [26] was excellent, not only in terms of the bond lengths of the NiNNNi core (NiN ~ 1.828 Å (calcd), 1.830 and 1.835 Å (expt.); NN ~ 1.124 Å (calcd), 1.121 Å (expt.)), but in reproducing more subtle aspects such as the T-shaped distortion at the nickel ($N_{\beta dik}$–Ni–N ~ 160° (154°, expt.) and 104° (108°, expt.)). The present (B3LYP/6-311+) calculations concur with the DFT calculations reported by these same researchers (B3LYP/6-31 G*) and Evans method magnetic susceptibility experiments [26].

Lastly, the optimized side-on ^{1}[Cu]–(η^2–N_2)–[Cu] complex (figure 6d) displays approximate C_{2v} symmetry, where the butterfly angle is 106.16° and each plane of the central Cu_2N_2 unit is coplanar with its respective β-diketiminate plane. The N–N bond lengths in the Cu end-on (1.119 Å) and side-on (1.167 Å) isomers are similar to those of the corresponding Ni complexes, even though the isomerization enthalpy of 13.3 kcal mol^{-1} is smaller by 5.3 kcal mol^{-1}.

In terms of N_2 activation, late transition metal [M]–NN–[M] complexes can be divided into two groups, irrespective of isomer: (i) Fe and Co complexes that have large and mutually similar N–N bond lengths that show a marked decrease on moving to (ii) Ni and Cu complexes. As the similar N_2 bond lengths of the end-on isomers in group (i) were accounted for in reference [24], it seems likely that an electronic explanation underlies the similarities in group (ii) for the corresponding end-on isomers. On the other hand, even though the N–N bond lengths in the side-on N_2 complexes follow the same trend, an electronic structure-based explanation is more elusive in light of their geometric disparity (*cf.* figure 6).

In considering monometallic [M]–N_2 and bimetallic [M]–N_2–[M] complexes, N_2 is more activated in the latter (*cf.* figures 1 and 3) for the entire 3-D series (Sc–Cu), a result that demonstrates the concerted nature of transition metals in weakening N_2. Additionally, the η^2–N_2 isomers display greater N_2 activation than κ^1–N_2 for each complex, supporting the MacLachlan–Fryzuk hypothesis [10]. Comparing early and late TM complexes, the more activated η^2–N_2 mode in bimetallic complexes is

thermodynamically stable for early metals (Sc–Cr; figure 3), whereas late transition metal systems (Fe–Cu) exhibit greater stability in their less-activated κ^1-N_2 isomers. Finally, while the trend of greater activation with earlier monometallic TM complexes is valid only in two subsets of the 3-D series (Sc–Cr and Mn–Cu; figure 1) owing to the anomalous behavior of Mn, bimetallics exhibit this behavior on the *entire* set, with the exception of a small "spike" for ^{9}[Mn]–(η^2–N_2)–[Mn] (blue line in figure 3).

4. Conclusion

Several avenues in the ongoing computational study of first row transition metal dinitrogen complexes have been discussed. The η^2–N_2 isomers in β-diketiminate supported transition metal complexes are calculated to be more activated but less stable than their κ^1–N_2 counterparts for late transition metals, whereas the η^2–N_2 mode was most stable for the earliest systems (figure 1). Furthermore, among the monometallic complexes, analysis of Δ(N–N) reveals that upon complexation of free N_2, side-bound N_2 is 0.018–0.054 Å longer than analogous end-bound N_2. These observations support the MacLachlan–Fryzuk hypothesis [10]. Moreover, the trends discussed here mimic and extend the prescient remarks by Himmel and Reiher [27] for N_2 interaction with bare 3-D metal atoms, reasonably implying that the metal plays the dominant role in the activation of dinitrogen with a subordinate role from the ligand, as we implied in our previous research. Although the same isomeric preferences across the 3-D series were calculated for bimetallic N_2 complexes (figure 3) as for monometallic complexes, the N–N bond lengths and hence N_2 activation, this study demonstrates that a useful starting point for activated dinitrogen complexes in furtherance of reactivity studies is the choice of *bimetallic* supporting ligands, which unlike monometallic ligands allow both metals to activate N_2 in a concerted fashion. For 3-D metals, the N_2 activation trends in bimetallic [M]–NN–[M] complexes more or less mirror those for their monometallic counterparts ([M]–N_2; figure 1). The manganese complexes are a noticeable but interesting exception to the foregoing characterization, and thus warrant closer experimental and computational scrutiny.

4.1. *Computational methods*

All calculations were performed upon neutral species using the Gaussian 09 suite of programs [28] with (unless noted otherwise) the B3LYP hybrid density functional methods [29]. The B3LYP/6-311+G(d) level of theory was used for all calculations reported herein except where noted. Optimized geometries and transition states were confirmed by the presence of zero and one imaginary frequencies, respectively, in the calculated energy Hessian. Thermochemistry was determined at 298.15 K and 1 atm using unscaled B3LYP/6-311+G(d) vibrational frequencies. Ground state spin multiplicities for each species are indicated in superscript (e.g., "^{3}[Sc]–N_2" for triplet [Sc]–N_2) and excited states with an asterisk (e.g., "^{4}[Ti]–(η^2–N_2)*" for excited-state quartet [Ti]–(η^2–N_2)).

Acknowledgments

The authors acknowledge the continued financial support from the National Science Foundation (CHE-0701247). AWP acknowledges the UNT Toulouse Graduate School for a College of Arts and Sciences Graduate Research Fellowship.

References

[1] C.E. Housecroft, A.G. Sharpe. *Inorganic Chemistry*, 2nd Edn, Pearson Prentice Hall, New York (2005).
[2] B.E. Smith. *Science*, **297**, 1654 (2002).
[3] M.P. Shaver, M.D. Fryzuk. *Adv. Synth. Catal.*, **345**, 1061 (2003).
[4] (a) R.R. Schrock. *Acc. Chem. Res.*, **38**, 95562 (2005); (b) R.R. Schrock. *Chem. Commun.*, **19**, 2389 (2003); (c) D.V. Yandulov, R.R. Schrock. *Science*, **301**, 76 (2003).
[5] D.A. Hall, G.J. Leigh. *J. Chem. Soc., Dalton Trans.*, **17**, 3539 (1996).
[6] (a) M.W. Schmidt, M.S. Gordon. *Ann. Rev. Phys. Chem.*, **49**, 233 (1998); (b) M.S. Gordon, M.W. Schmidt, G.M. Chaban, K.R. Glaesemann, W.J. Stevens, C. Gonzalez. *J. Chem. Phys.*, **110**, 4199 (1999).
[7] J.M. Smith, A.R. Sadique, T.R. Cundari, K.R. Rodgers, G. Lukat-Rodgers, R.J. Lachicotte, C.J. Flaschenreim, J. Vela, P.L. Holland. *J. Am. Chem. Soc.*, **128**, 756 (2006).
[8] A.D. Allen, C.V. Senoff. *Chem. Commun.*, 621 (1965).
[9] W.J. Evans, T.A. Ulibarri, J.W. Ziller. *J. Am. Chem. Soc.*, **110**, 6877 (1998).
[10] E.A. MacLachlan, M.D. Fryzuk. *Organometallics*, **25**, 1530 (2006).
[11] F.H. Allen, J.E. Davies, J.J. Galloy, O. Johnson, O. Kennard, C.F. Macrae, E.M. Mitchell, G.F. Mitchell, J.M. Smith, D.G. Watson. *J. Chem. Inf. Comput. Sci.*, **31**, 187 (1991).
[12] D. Rehder, C. Woitha, W. Priebsch, H. Gailus. *Chem. Commun.*, 364 (1992).
[13] J.E. Salt, G.S. Girolami, G. Wilkinson. *J. Chem. Soc., Dalton Trans.*, 685 (1985).
[14] C. Perthuisot, M. Fan, W.D. Jones. *Organometallics*, **11**, 3622 (1992).
[15] R. Waterman, G.L. Hillhouse. *Can. J. Chem.*, **83**, 328 (2005).
[16] R.L. Collin, W.N. Lipscomb. *Acta Cryst.*, **4**, 10 (1951).
[17] S.F. Sousa, P.A. Fernandes, M.J. Ramos. *J. Phys. Chem. A*, **111**, 10439 (2007).
[18] (a) A.D. Becke. *J. Chem. Phys.*, **104**, 1040 (1996); (b) A.D. Becke. *J. Chem. Phys.*, **98**, 1372 (1993). (c) A.D. Becke. *J. Chem. Phys.*, **98**, 5648 (1993).
[19] G.K.B. Clentsmith, V.M.E. Bates, P.B. Hitchcock, G.N. Cloke. *J. Am. Chem. Soc.*, **121**, 10444 (1999).
[20] M. Carlotti, J.W.C. Johns, A. Trombetti. *Can. J. Phys.*, **52**, 340 (1974).
[21] W.H. Monillas, G.P.A. Yap, L.A. MacAdams, K.H. Theopold. *J. Am. Chem. Soc.*, **129**, 8090 (2007).
[22] W.A. Chomitz, J. Arnold. *Chem. Commun.*, 4797 (2007).
[23] P.L. Holland. *Acc. Chem. Res.*, **41**, 905 (2008).
[24] K. Ding, A.W. Pierpont, W.W. Brennessel, G. Lukat-Rodgers, K.R. Rodgers, T.R. Cundari, P.L. Holland. *J. Am. Chem. Soc.*, **131**, 9471 (2009).
[25] J.M. Smith, R.J. Lachicotte, K.A. Pittard, T.R. Cundari, K.R. Lukat-Rodgers, K.R. Rodgers, P.L. Holland. *J. Am. Chem. Soc.*, **123**, 9222 (2001).
[26] (a) S. Pfirrmann, S. Yao, B. Ziemer, R. Stösser, M. Driess, C. Limberg. *Organometallics*, **28**, 6855 (2009); (b) S. Pfirrmann, C. Limberg, B. Ziemer. *Dalton Trans.*, 6689 (2008); (c) S. Pfirrmann, C. Limberg, C. Herwig, R. Stößer, B. Ziemer. *Angew. Chem. Int. Ed.*, 48, 3357 (2009).
[27] H.-J. Himmel, M. Reiher. *Angew. Chem. Int. Ed.*, 45, 6264 (2006). See also M. Reiher. *Nachr. Chem.*, 57, 1093 (2009).
[28] M.J. Frisch, G.W. Trucks, H.B. Schlegel, G.E. Scuseria, M.A. Robb, J.R. Cheeseman, G. Scalmani, V. Barone, B. Mennucci, G.A. Petersson, H. Nakatsuji, M. Caricato, X. Li, H.P. Hratchian, A.F. Izmaylov, J. Bloino, G. Zheng, J.L. Sonnenberg, M. Hada, M. Ehara, K. Toyota, R. Fukuda, J. Hasegawa, M. Ishida, T. Nakajima, Y. Honda, O. Kitao, H. Nakai, T. Vreven, J.A. Montgomery Jr, J.E. Peralta, F. Ogliaro, M. Bearpark, J.J. Heyd, E. Brothers, K.N. Kudin, V.N. Staroverov, R. Kobayashi, J. Normand, K. Raghavachari, A. Rendell, J.C. Burant, S.S. Iyengar, J. Tomasi, M. Cossi, N. Rega, J.M. Millam, M. Klene, J.E. Knox, J.B. Cross, V. Bakken, C. Adamo, J. Jaramillo, R. Gomperts, R.E. Stratmann, O. Yazyev, A.J. Austin, R. Cammi, C. Pomelli, J.W. Ochterski, R.L. Martin, K. Morokuma, V.G. Zakrzewski, G.A. Voth, P. Salvador, J.J. Dannenberg, S. Dapprich, A.D. Daniels, Ö. Farkas, J.B. Foresman, J.V. Ortiz, J. Cioslowski, D.J. Fox. *Gaussian 09*, Revision A.1; Gaussian, Inc., Wallingford, CT (2009).
[29] A.D. Becke. *Phys. Rev. A*, **38**, 3098 (1988).